# On calculating the magnetic state of nanostructures

G. Malcolm Stocks [a,*], M. Eisenbach [a], B. Újfalussy [b],
B. Lazarovits [c], L. Szunyogh [d], P. Weinberger [c]

[a] *Materials Science and Technology Division, Oak Ridge National Laboratory, P.O. Box 2008-6114,
Oak Ridge, TN 37831-6114, United States*
[b] *Institute for Solid State Physics, H-1525 Budapest, P.O. Box 49 H-1525, Hungary*
[c] *Center for Computational Materials Science, Technical University Vienna, A-1060, Gumpendorferstr.
1.a., Vienna, Austria*
[d] *Department of Theoretical Physics and Center for Applied Mathematics and Computational Physics,
Budapest University of Technology and Economics, Budafoki út 8, H-1111 Budapest, Hungary*

## Abstract

We review some of our recent work on first principles calculations of the magnetic structure of surface and bulk nanostructures. The calculations are based on implementation of relativistic density functional theory within state of the art surface embedding and order-$N$ multiple scattering Green's function methods. First principles spin-dynamics and the constrained local moment approximation are reviewed as they relate to optimization of moment configurations in highly inhomogeneous materials such as surface and bulk nanostructures. Results are present for three prototypical nanostructures – short Co-chains adjacent to a Pt{111}-surface step-edge, a Cr-trimer on the Au{111}-surface, and Fe-chains and impurities in Cu – that illustrate the need to treat the underlying electronic interactions on a fully self-consistent basis in which the very different energy scales appropriate to exchange coupling and magneto-crystalline anisotropy are treated on an equal footing.
© 2006 Published by Elsevier Ltd.

* Corresponding author. Tel.: +1 865 5745763; fax: +1 865 5747659.
*E-mail addresses:* stocksgm@ornl.gov (G.M. Stocks), eisenbachm@ornl.gov (M. Eisenbach), bu@szfki.hu (B. Újfalussy), bl@szfki.hu (B. Lazarovits), szunyogh@phy.bme.hu (L. Szunyogh), pw@cms.tuwien.ac.at (P. Weinberger).

**Contents**

## 1. Introduction

Driven by the need for ever higher density recording media, smaller and more responsive sensors, and higher energy product permanent magnets, *nanomagnetism*, the science and technology of nanoscale magnetic materials and devices, is currently one of the focii of nanoscience research [1]. A fundamental problem in understanding nanoscale magnetic phenomena is that it is generally not possible to construct simple models based on parameters obtained for bulk systems – neither experimentally nor theoretically. Furthermore, experimental characterization of nanoscale features is also often problematical without sophisticated theory and modelling to interpret experimental results.

Modelling of magnetic properties is an example of a complex multiscale problem of a type long championed by Professor Pettifor where different models are applied at different length scales, from the electronic quantum scale where moment formation occurs, to the atomistic scale where Heisenberg and related spin models are appropriate, to the device level where it is often sufficient to describe the magnetic state and moment dynamics using continuum micromagnetics methods [2].

The phenomenological theory of moment or spin dynamics (SD) is encapsulated in the well-known Landau–Liftshitz–Gilbert equation (LLG) equation [3–5,2]

$$\frac{\delta}{\delta t}\vec{m} = -\gamma \vec{m} \times \vec{H}^{\text{eff}} + \frac{\lambda}{m}\vec{m} \times \{\vec{m} \times \vec{H}^{\text{eff}}\} \tag{1}$$

where $\gamma$ is the gyromagnetic ratio and $\lambda$ is the Gilbert damping factor and the effective forcing field $\vec{H}^{\text{eff}} = \delta E(\vec{m})/\delta \vec{m}$ is obtained from the derivative of the internal energy $E(\vec{m})$ with respect to the moment $\vec{m}$. For application purposes it is often useful to decompose $\vec{H}^{\text{eff}}$ into a series of terms

$$\vec{H}^{\text{eff}} = \vec{H}^{\text{extern}} + \vec{H}^{\text{exch}} + \vec{H}^{\text{anis}} + \vec{H}^{\text{dipole}} + \vec{H}^{\text{elast}} \tag{2}$$

which from left to right, correspond to contributions from applied external fields, intrinsic exchange interactions, magneto crystalline anisotropy, dipolar interactions, and magneto-elastic effects. Although the LLG equation is extremely valuable in simulations, particularly

in device physics, where it provides the basis for modern industrial micromagnetics simulations, the fact that its microscopic underpinning is not well formulated makes it of much less value at the nanoscale. Indeed, at the nanoscale the discretised elements of material to which magnetic moments and their interactions are assigned necessarily approach atomic dimension and it becomes necessary to treat the underlying atomistic nature of the magnetic moments and their interactions.

Although, at an intermediate scale, Heisenberg and related spin models can be used, this does not aid with the fundamental issue of how to determine the parameters of such a model (exchange interactions, $J_{ij}$, anisotropy constants $K_i$, ...) in small, highly inhomogeneous systems. Clearly, these considerations demand theory and modeling techniques that can deal with the quantum nature of the atomic scale interactions while still being able to deal with the complexity and inhomogeneity of realistic models of nanostructures. Here modern first principles density functional theory (DFT) based electronic structure methods have progressed to the stage where this is increasingly practicable [6–8].

In general, spin structures result from a subtle interplay between the exchange interaction, which normally determines the magnetic order, and the spin–orbit interaction, which couples the spin to the lattice and gives rise to the magneto-crystalline anisotropy energy (MAE). As a result the magnetic structure – magnetic moments, non-collinearity, magnetic anisotropy – can only be fully discussed within the framework of relativistic electron theory [9]. In the remainder of this paper we discuss results of some of our recent calculations that address magnetic structure of prototypical nanostructures using first principles electronic structure methods. In the next section, we outline fully relativistic DFT as the vehicle for treating the quantum mechanical interactions that determine the magnetic structure. In particular allowing for treatment of exchange and magneto-crystalline anisotropy within a unified electronic framework. First principles spin dynamics and the constrained local moment model of non-equilibrium moment configurations is discussed in Section 2.2. A brief description of the first principles multiple scattering theory Greens function codes for performing calculation for surface [10,11] and bulk [8] nanostructures in which these techniques are implemented is given in Section 2.3. In Section 3, we present results for three prototypical nanostructures – short Co-chains adjacent to a Pt{111}-surface step-edge (Section 3.1), a Cr-trimer on the Au{111}-surface (Section 3.2), and Fe-chains and impurities in Cu (Section 3.3) – that highlight the need for using such first principles electronic structure techniques when dealing with the inhomogeneities inherent to nanostructures. Section 4 contains some concluding remarks.

## 2. Computational methods for magnetic nanostructures

### 2.1. Relativistic density functional theory

The calculations discussed in the following sections are based on first principles DFT [16,17] in the local spin density approximation (LSDA) [18]. A detailed presentation of relativistic DFT is given by Dreizler and Gross [19], here we only review the main results as they apply to our relativistic treatment of magnetic systems. A fully relativistic extension of DFT leads to a current density functional [20–22] where the energy functional takes the form

$$E[j^{\mu}] = \int^{E_f} \epsilon n(\epsilon)\,\mathrm{d}\epsilon - \frac{e^2}{2} \iint \frac{j_{\mu}(\vec{r})j^{\mu}(\vec{r}')}{|\vec{r} - \vec{r}'|}\,\mathrm{d}^3r\,\mathrm{d}^3r' + E_{xc}[j^{\mu}(\vec{r})]$$
$$- \int \frac{\delta E_{xc}[j^{\nu}]}{\delta j^{\mu}(\vec{r})} j^{\mu}(\vec{r})\,\mathrm{d}^3r \tag{3}$$

where $j_{\mu}(\vec{r})$ is the four-current. This expression can be reformulated in terms of the charge and magnetisation densities [23] using the Gordon decomposition. When the orbital current densities are neglected the form of the functional becomes identical to the non-relativistic spin density functional

$$E[n, \vec{m}] = \int^{E_f} \epsilon n(\epsilon)\,\mathrm{d}\epsilon - \frac{e^2}{2} \iint \frac{n(\vec{r})n(\vec{r}')}{|\vec{r} - \vec{r}'|}\,\mathrm{d}^3r\,\mathrm{d}^3r' + E_{xc}[n, \vec{m}]$$
$$- \int \frac{\delta E_{xc}[n, \vec{m}]}{\delta n(\vec{r})} n(\vec{r})\,\mathrm{d}^3r - \int \frac{\delta E_{xc}[n, \vec{m}]}{\delta \vec{m}(\vec{r})} \vec{m}(\vec{r})\,\mathrm{d}^3r \tag{4}$$

where the Kohn–Sham orbitals are now obtained as solutions of the Kohn–Sham-Dirac equation

$$(-\mathrm{i}\hbar c\vec{\alpha} \cdot \vec{\nabla} + \beta mc^2 + V^{\mathrm{eff}}(\vec{r}) + \beta\vec{\sigma} \cdot \vec{B}^{\mathrm{eff}}(\vec{r}) - \epsilon_i)\psi_i = 0 \tag{5}$$

in which the interaction of the orbital current with the vector potential is excluded. In this equation the effective potential $V^{\mathrm{eff}}$ and magnetic field $\vec{B}^{\mathrm{eff}}$ are given by

$$V^{\mathrm{eff}}(\vec{r}) = V^{\mathrm{ext}}(\vec{r}) + e^2 \int \frac{n(\vec{r})}{|r - r'|}\,\mathrm{d}^3r' + \frac{\delta E_{xc}[n, \vec{m}]}{\delta n}(\vec{r}) \tag{6}$$

and

$$\vec{B}^{\mathrm{eff}}(\vec{r}) = \vec{B}^{\mathrm{ext}}(\vec{r}) + \frac{\delta E_{xc}[n, \vec{m}]}{\delta \vec{m}}(\vec{r}) \tag{7}$$

respectively. Using the standard definition of the Green function $G(\vec{r}, \vec{r}'; \epsilon) = \lim_{\eta \to 0} \sum_i \psi_i^{\dagger}(\vec{r})\psi_i(\vec{r}')/(\epsilon_i - \epsilon + \mathrm{i}\eta)$ the density of states $n(\epsilon)$, the charge density $n(\vec{r})$, and the magnetisation density $\vec{m}(\vec{r})$ can then be written as

$$n(\epsilon) = \frac{1}{\pi}\mathrm{Im} \int \mathrm{Tr}\, G(\vec{r}, \vec{r}; \epsilon)\,\mathrm{d}^3r \tag{8}$$

$$n(\vec{r}) = \frac{1}{\pi}\mathrm{Im} \int^{E_f} \mathrm{Tr}\, G(\vec{r}, \vec{r}; \epsilon)\,\mathrm{d}\epsilon \tag{9}$$

$$\vec{m}(\vec{r}) = \frac{1}{\pi}\mathrm{Im} \int^{E_f} \mathrm{Tr}\, \vec{\sigma}G(\vec{r}, \vec{r}; \epsilon)\,\mathrm{d}\epsilon \tag{10}$$

Taken together, Eqs. (5)–(10) define a a set of (relativistic) self-consistent field equations for determining the ground state charge and magnetization densities and together with Eq. (4) the total energy.

In principle, these equations allow the calculation of any magnetic state that is an extremum of the energy functional. This is particularly important for calculating the magneto-crystalline anisotropy energy, $E_{\mathrm{MAE}}$, as the difference

$$E_{\mathrm{MAE}} = E(\vec{m}_1) - E(\vec{m}_2) \tag{11}$$

where $E(\vec{m}_1)$ and $E(\vec{m}_2)$ are the LSDA-energies for the two orientations of the magnetization, $\vec{m}_1$ and $\vec{m}_2$, corresponding to the easy and hard directions. Clearly, the easy direction refers to a minimum (actually the global minimum) of the LSDA energy functional which standard iterative approaches to solving the LSDA equations can be expected to find. On the other hand, the hard direction corresponds to a maximum of the functional with respect to the magnetization, in fact the global maximum. While for high symmetry systems, candidates for the hard direction are simple to obtain, for highly inhomogeneous nanostructures this may not be the case. This situation is further complicated by the fact that iteration from some guess that is not precisely a maximum will generally result in the solution to the LSDA equations running towards the closest local minimum. In Section 2.2, we outline a method to overcome this difficulty using the constrained local moment approach.

Magneto-crystalline anisotropy energies are typically very small and are notoriously difficult to calculate from the subtraction of the (large) total energies corresponding to independent self-consistent LSDA calculations as in Eq. (11). Thus, it is common to approximate the MAE as the difference in band structure energies, namely,

$$E_{\text{MAE}} = E_{\text{BS}}(\vec{m}_1) - E_{\text{BS}}(\vec{m}_2) \tag{12}$$

where the band structure energy is simply the first term on the right hand side of the LDA energy functional, namely,

$$E_{\text{BS}}(\vec{m}_i) = \int_{-\infty}^{\varepsilon_{\text{F}}(\vec{m}_i)} n(\varepsilon; \vec{m}_i) \, \mathrm{d}\varepsilon \tag{13}$$

This approximation is the result of using magnetic force theorem (MFT) [12] or frozen potential approximation (FPA) [13,14] and involves performing a fully self-consistent LSDA calculation for only one of the magnetization directions (say the easy direction) and then using the LSDA potentials for this orientation in a single shot calculation (a single evaluation of Eq. (5)) for the second with subsequent subtraction of the (much smaller) band structure energies (Eq. (12)).

## 2.2. First principles spin dynamics

The formalism developed in the previous section is valid for the ground state only and does not provide any mechanisms for addressing moment dynamics in a manner equivalent to the LLG-equation. The foundation for a first principles spin-dynamics of itinerant
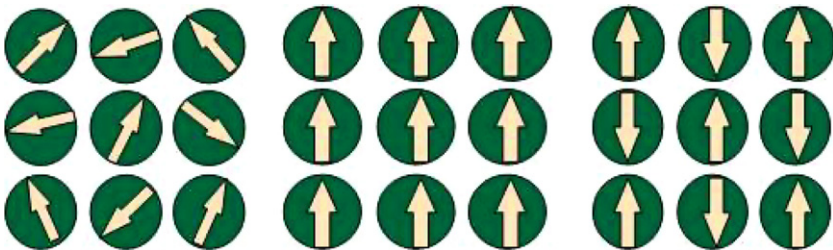


Fig. 1. Illustration of general local moment state $\{\vec{e}_i\}$ (left). Example ferromagnetic (FM) and antiferromagnetic (AFM) states (center and right) are specified by $\vec{e}_i = (0,0,1)$ for all sites (FM) and $\vec{e}_i = (0,0,1)$ or $(0,0,-1)$ depending on whether the particular site moment is *up* or *down* (AFM).

electron systems was set out by Antropov et al. [24,25], and was later expanded upon by others [26–28]. The basic assumption underlying first principles spin dynamics (FP-SD) is that it is useful to divide moment dynamics according to two different time scales; a fast, *electronic*, time-scale responsible for the formation of a well defined local, atomic like, moment at each site and a slow, reorientational, time-scale upon which the preformed local moments turn rigidly [29]. This is illustrated in the leftmost frame of Fig. 1 where, within some volume about the *i*th atomic site, the local moment points in the direction of the unit vector $\vec{e}_i = \int_{\Omega_i} \vec{m}_i(\vec{r})\, d\vec{r} / |\int_{\Omega_i} \vec{m}_i(\vec{r})\, d\vec{r}|$ and a general orientational configuration can be specified by a set of such vectors $\{\vec{e}_i\}$. The corresponding moment configuration is then $\{\vec{m}_i\}$ with $\vec{m}_i = m_i\vec{e}_i$ where $m_i = |\vec{m}_i|$. The central result of FP-SD is that, for the precessional component of the motion, the evolution of the time dependent moment configuration, $\{\vec{m}_i\}$, is described by a microscopic, quasi-classical equation of motion which is exactly of the form as the classical LL-equation; namely, the first term on the RHS of Eq. (1) but now with an effective field, $\vec{B}_i^{\mathrm{eff}}$, that is based on first principles theory. Specifically,

$$\frac{\delta}{\delta t}\vec{m}_i = -\gamma \vec{m}_i \times \vec{B}_i^{\mathrm{eff}} \tag{14}$$

with

$$\vec{B}_i^{\mathrm{eff}}(\{\vec{m}_j\}) = \delta E^{\mathrm{LSDA}}(\{\vec{m}_j\})/\delta \vec{m}_i \tag{15}$$

where $E^{\mathrm{LSDA}}(\{\vec{m}_i\})$ is the LSDA energy obtained by solving the LSDA equations for the instantaneous state $\{\vec{m}_i\}$. Thus FP-SD is very much an equivalent for the local moment dynamics of first principles molecular dynamics (FP-MD) for atomic motion with the obvious caveat that the separation of times scales between the electronic degrees of freedom that determine the forces in FP-MD and the slow nuclear motion which is governed by Newton's equations is much cleaner that in the case of moment dynamics where there is no equivalent of Born–Oppenheimer approximation for local moments.

Compared to FP-MD, there is a second problem to be faced by FP-SD. This results from the fact that DTF is specifically geared to finding the total energy (and forces) corresponding to a fixed external potential, which, for FP-MD, is fully specified once the atomic positions are given, for local moments there is no such external potential. For the spins, solutions to the LSDA equations, in both relativistic and non-relativistic forms, correspond only to extrema; normally some fairly simple ferromagnetic (FM) or antifer-romagnetic (AFM) ground state of the type visualized in the two rightmost two frames of Fig. 1. In particular, LSDA is silent on a general orientational configuration $\{\vec{e}_i\}$ of the type visualized in the leftmost frame of Fig. 1. Furthermore, any attempt to iterate the standard LSDA equations starting from such a configuration will result in the solution, once again, running towards the nearest local minimum, e.g. a nearby FM or AFM state. Thus, in order to have a theory for $E^{\mathrm{LSDA}}(\{\vec{m}_i\})$, it is necessary to go beyond conventional LSDA theory for the ground state. This same conclusion was reached by Capelle et al. [27] in their work to derive FP-SD by taking the adiabatic limit of time dependent DFT [27].

A technique to deal with such a general state has been presented by Stocks et al. [30,31] based on the constrained density functional theory developed by Dederich et al. [32]. In the constrained local moment (CLM) model the LSDA equations are solved subject to a constraint

$$\int_{\Omega_i} \vec{m}_i(\vec{r}) \times \vec{e}_i \, d\vec{r} = 0 \tag{16}$$

that ensures that the local magnetizations lay along the directions prescribed by $\{\vec{e}_i\}$. The result is that, in order to maintain the specific orientational configuration, a local transverse constraining field must be applied at each site the effect of which is to kill components of the magnetization transverse to $\vec{e}_i$. The constraining field is obtained from the condition

$$\frac{\delta E^{con}[\{\vec{e}_i\}, \{\vec{B}_i^{con}\}]}{\delta \vec{e}_i} = 0 \tag{17}$$

applied to all sites and where $E$ the generalized energy functional in the presence of the constraining field

$$E^{con}[\{\vec{e}_i\}, \{\vec{B}_i^{con}\}] = E^{int}[\{\vec{e}_i\}, \{\vec{B}_i^{con}\}] + \int d\vec{r} \vec{M}(\vec{r}) \cdot \vec{B}(\vec{r}) \tag{18}$$

This formalism can be made into a practical computational algorithm by choosing $B_i^{con}(\vec{r})$ to be of the functional form

$$B_i^{con}(\vec{r}) = B_{xc}^i(\vec{r}) \vec{c}_i \tag{19}$$

where $B_{xc}^i(\vec{r})$ is the local (longitudinal) exchange correlation potential at the site $i$ and $\vec{c}_i$ is a unit vector normal to local orientation $\vec{e}_i$. That Eq. (19) is a good approximation for the constraining field can be monitored a posteriori by checking the extent to which the transverse components of $m_i(\vec{r})$ are quenched.[1] Coupled with an efficient iterative algorithm for finding the constraining field, [31], the above equations provide a straightforward way to obtain the energy and constraining fields associated with any non-equilibrium CLM state. Of course the standard LSDA ground states are simply CLM states for which $B_i^{con} = 0$ at all sites.

To make the connection between the CLM model and FP-SD it is sufficient to note that the internal effective field that rotates the spins is just the opposite of the constraining field, i.e. Eq. (15) in $\mathbf{B}_i^{eff} = -\mathbf{B}_i^{con}$. Although implied by use of Eq. (15) with Eq. (14), we do not include a torque coupling the spin and orbital degrees of freedom. As pointed out by Antropov et al. [25], this is only applicable when the deviation between the orientations of the spin and orbital moments is small.

As set out Eq. (14) only takes care of the precessional motion of the moment and the equivalent of the Gilbert term does not occur. Some ideas about how to include such a term have been given by Capelle and Györffy [28], here however we are only interested in FP-SD as a devise for finding the ground state it is sufficient to add Gilbert damping phenomenologically as

$$\frac{\delta}{\delta t} \vec{m}_i = -\gamma \vec{m}_i \times \vec{B}_i^{eff} + \alpha \vec{m}_i \times [\vec{m}_i \times \vec{B}_i^{eff}] \tag{20}$$

where $\alpha$ is an constant that can be adjusted to ensure rapid convergence to the ground state (or, at least, the nearest local minimum).

---

[1] Studies of the residual transverse moments of Fe in various non-equilibrium situations reveal that they are typically reduced by 2–3 orders of magnitude by the application of this form of constraint.

*2.3. Multiple scattering theory Green's function methods*

To solve the LSDA equations, we use multiple scattering theory (MST) [33,34], or Korringa, Kohn and Rostoker (KKR) [35,36], Green's function (GF) approaches tailored to deal with realistic models of nanostructures. Specifically, we use two different implementations of relativistic MST one appropriate to isolated nanostructures on metal surfaces and one for nanostructures embedded in bulk materials. Both codes treat non-collinear magnetism, CLM states and use of damped FP-SD (Eq. (20)) to find complex magnetic ground state structures. It is important note that in both of these methods we can control the convergence and numerical precision of the solutions of the LSDA equations to a degree that allows to directly compute magneto-crystalline anisotropy and to find the easy direction using the CLM model and FP-SD.

To treat surface nanostructures, we use the Green's function embedded cluster (GF-EC) method developed by Lazarovits et al. [11]. An important advantage of this method is that an isolated nanostructure placed on an otherwise semi-infinite surface is modelled directly; as opposed supercell approaches where some artificial periodicity and, consequently, interactions is introduced. Use of the GF-EC method involves two distinct steps. Firstly, a self-consistent calculation for the pristine surface system is performed using the relativistic Screened-KKR method [10]. The nanostructure (or extended impurity) is subsequently *embedded* into this host using standard MST embedding techniques [11]. Of course to treat the interaction between the nanostructure and the surface the *extended impurity* that is actually treated self-consistently consists of the actual nanostructure plus surrounding surface and subsurface atoms and vacuum sites as appropriate [7].

To treat nano-structures embedded in bulk materials we deploy a fully relativistic (Rel-LSMS) version of the Locally Self-consistent Multiple Scattering (LSMS) approach. In the Rel-LSMS method the Kohn–Sham-Dirac equation (Eq. (5)) is solved rather than the corresponding non(semi)-relativistic Schrödinger equation of the original technique [37]. The Rel-LSMS method has basically the same order-N scaling properties of the original and is therefore capable of treating the large numbers of atoms needed to model nanostructures while being able to obtain total energies, and consequently charge and magnetization densities, converged to the high degree of numerical precision required to treat anisotropy.

## 3. Calculated magnetic structure of nano-structures

In this section we present results of first principles calculations of the ground state magnetic structure for some prototypical nanostructures using the techniques outlined above. Specifically, we discuss three nanostructures, namely, short Co-chains adjacent to a Pt{111}-surface step-edge [6], a Cr-trimer on the Au{111}-surface, and Fe-chains and impurities in Cu. Taken together these examples illustrate the need to treat the underlying electronic interactions on a fully self-consistent basis in which the very different energy scales appropriate to exchange coupling ($\sim$1 mRy) and magneto-crystalline anisotropy ($\sim$1 $\mu$Ry) are treated on an equal footing.

*3.1. Co-chains at a Pt[111]-surface step*

In a recent *Nature* article, Gambardella et al. [38,39] reported the results of experiments on well characterized finite linear chains of Co atoms located at a step edge of a Pt(111)
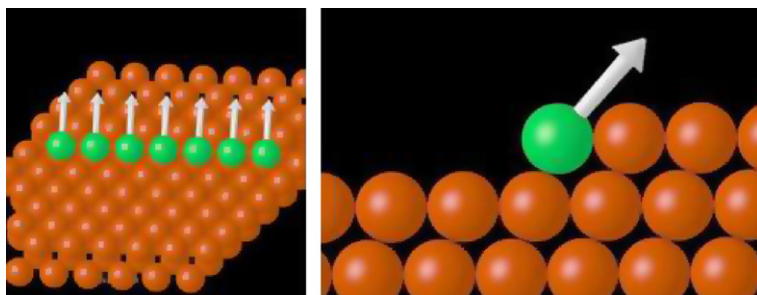
Fig. 2. Moment orientations for Co-atoms at a Pt-(1 1 1) step-edge. Left: Oblique view to illustrate collinearity of Co-moments. Right: Edge view to illustrate the tilt of the ferromagnetically ordered Co-moments towards the Pt-step edge.

surface terrace. At 45 K the formation of ferromagnetic spin-blocks of about 15 atoms was observed with an easy magnetization axis normal to the chain and pointing along a direction of 43° towards the step edge. This surprising result is not readily understood it terms of either simple symmetry considerations or spin models and, presumably, arises from the details of the electronic interactions of the Co atoms with the Pt-step edge.

In Fig. 2 we show, in the left panel, a visualization of the results of our first principles calculations of a 7-atom Co-chain adjacent to a 111-Pt step-edge using the GF-EC cluster approach outlined above [7]. As can been seen the Co moments align ferromagnetically and are almost collinear, with a maximum deviation of <1°, and cant at an angle of 42° towards the step edge – in quantitative agreement with the experiments of Gambardella [38].

The calculations were performed using the GF-EC method describe above. Computationally the Co-chain together with the Pt-step was treated as an extended impurity embedded in a trough in an otherwise perfect semi-infinite Pt-surface (for details of the model see Ref. [7]). Constrained density functional theory was used to calculate the magnetic state at each time step in the evolution of Eq. (20) as the moments were relaxed towards equilibrium. In the calculations only the damping term was included during the integration of Eq. (20).

In Fig. 3 we show a visualization of the evolution of the moment orientations (the fictitious moment dynamics) for 4 time-steps ($t = 1$, $t = 10$, $t = 25$ and $t = 100$) in the FP-SD optimization. As can been from the leftmost frame of this figure, the Co-moments were initialized to point along the step-edge.[2] To obtain good converge for the ground state moment configuration took a total of 800 time-steps, thus the visualizations shown in Fig. 3 show only the short time behavior. As emphasized earlier because the calculations were fully relativistic, the large exchange interactions and much smaller magneto-crystalline anisotropy energy were treated on the same footing. Thus, what is being seen in Fig. 3 is the effect of the large, exchange interaction dominated, energy scale as the moments snap into an over-all FM state. The subsequent slow relaxation of the FM-state from the positions shown in the rightmost from of Fig. 3 to the final positions of Fig. 2, which takes a further 700 time-steps, is reflective of the much smaller energy scale of the MAE.

---

[2] Addition calculations where the initial Co-moment configuration was chosen randomly produced the same ground state and had similar over-all behavior in terms of its convergence characteristics.
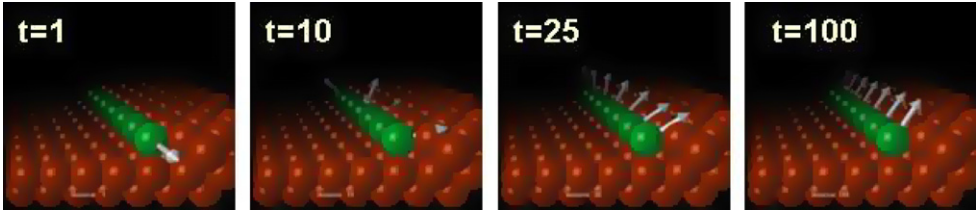
Fig. 3. Moment orientations for 4 time-steps in the LL-optimization of the magnetic structure of a 7-atom Co-chain adjacent to a 111-Pt step edge. From left to right the time steps are $t = 1$, $t = 10$, $t = 25$, $t = 100$.
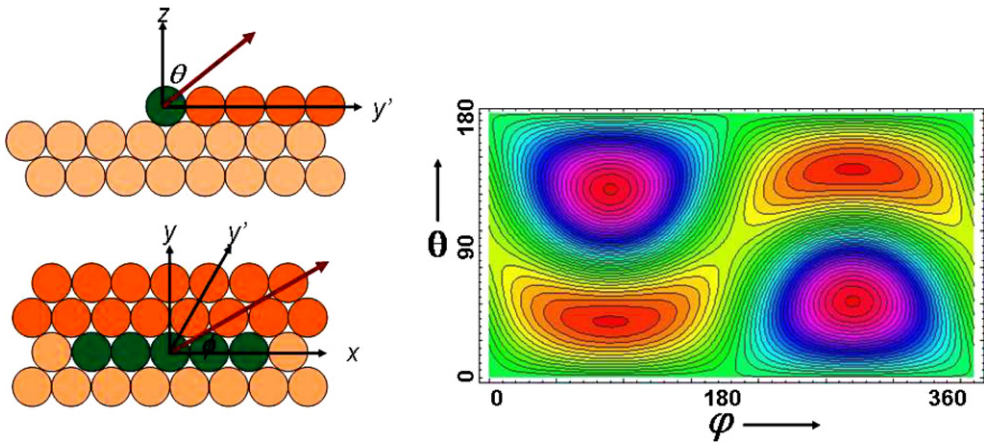


Fig. 4. Right-frame: Contour plot of the energy as a function of the orientation of the magnetization relative to the Co-Chain. Left-frame: Definition, relative to the Co-chain, of the angles $\theta$ and $\phi$ used in the contour plot; the upper component is a side elevation while the lower component is a plan view of the Co-chain (green) and the lower (low-density orange) and upper (high-density orange) terraces of the Pt-step. (For interpretation of the references to the color in this figure legend, the reader is referred to the web version of this article.)

Since the ground state is essentially collinear, studies of the energy of the system as a function of the orientation can be greatly simplified by studying the rotation of the global and uniform magnetization, $E(\theta, \phi)$ using the FPA. Fig. 4 (right-frame) is a contour plot of the energy as a function of the angles $\theta$, the angle the magnetization makes relative to the surface normal, and $\phi$, the same but relative to the step edge and in the Pt-surface (Fig. 4, left frame). These particular calculations are based on the potentials of the ground state obtained from the FP-SD optimization procedure. The full surface was obtained by calculating the energy for four (three plus the ground state) orientations of the magnetization and fitting the resulting energies to the functional form appropriate for the wire symmetry and expanded to second order in the anisotropy constants, namely [6]

$$E(\theta, \phi) = E_0 + K_{2,2}\cos 2\theta + K_{2,2}(1 - \cos 2\theta)\cos 2\phi + K_{2,3}\sin 2\theta \sin \phi \qquad (21)$$

where $K_{2,i}$, $i = 1, 2, 3$ are the three second order anisotropy constants. The calculated values are $K_{2,1} = -0.16$ meV, $K_{2,2} = -1.06$ meV, and $K_{2,3} = -4.81$ meV. From this fit the easy axis turns out to be $\theta = 38°$ and $\phi = 90°$, which is rather close to the one obtained from the FP-SD calculation, indicating that the FPA works rather well for this system.
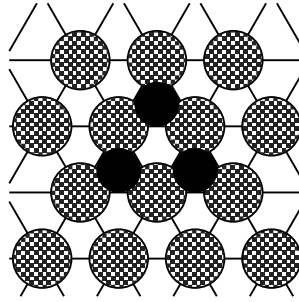
Fig. 5. Sketch of the atomic positions of a Cr trimer (full circles) on a Au(1 1 1) surface (shaded circles) used in the calculations.

Furthermore, the hard axis is obtained at $\theta = -52°$ and $\phi = 90°$, i.e., by $\Delta\theta = -90°$ away of the easy axis. This is again in good agreement with experiment [38]. Finally, $E_{MAE} = 1.42$ meV/Co-atom, once more in rather good agreement with the experimental estimate of 2 meV/Co-atom. From Fig. 4 it is clear that there is a meta-stable state at $\theta = 90°$ and $\phi = 0°$ which is $\Delta E = 0.33$ meV/Co-atom relative to the easy axis which implies a blocking temperature of $\sim 3.8$ K.

Before closing this section it should be noted that this system has been the subject of at least two other studies [40,41]. In these studies the full-potential linearized-augmented-plane-wave (FP-LAPW) method, including spin–orbit coupling, was used in conjunction with super-cell models of the Co-wire against the Pt-step-edge nanostructure. In the most recent and most detailed study, Baud et al. obtain very similar results to ours, provided they do not allow atomic relaxation (also neglected in our work). However, when relaxation is included the agreement worsens, this despite the fact that they are presumably improving the quality of the overall model. This suggests that the underlying LSDA may need improvement, perhaps by including orbital polarization effects.

## 3.2. Cr trimer on Au(1 1 1)

Antiferromagnetically coupled moments placed on a triangular lattice experience frustration which leads to the development of complex non-collinear magnetic orderings. Although the consequences of such frustration have been well-studied for localized spins by using Ising and Heisenberg model Hamiltonians [42,43] and more recently using first principles LSDA methods, it remains a subject of great interest [44–48]. Here we present results of a study of a close packed Cr-trimer on the Au(1 1 1) surface that displays these effects and illustrates the subtleties involved in uniquely determining the ground state. Although, DFT based ab-initio methods fail to describe strong electron correlation and hence Kondo effect that has been experimentally observed in this system[3] the Cr trimer

---

[3] It is important to note that, when the Cr atoms form an equilateral triangle, a sharp Kondo resonance of width $T_K \sim 50$ K ($T_K$ being the Kondo temperature) [49] was found in scanning tunneling microscopy (STM) signals. Consequently, at least at low temperatures, the system is subject of strong electron correlations that can be studied, e.g., in terms of renormalization group methods [50].

treated as an itinerant magnetic system provides an instructive case for first principles spin-dynamics studies of frustrated systems.

To study this system we have again used the relativistic ab-initio spin-dynamics and the GF-EC code to search for the ground state of a Cr trimer deposited on Au(111), see Fig. 5. For the positions of the Cr atoms and the underlying Au atoms we adopted the sites of the host Au fcc lattice, i.e., we neglected possible relaxations of the geometry. We started the simulations from arbitrary random directions of the Cr magnetic moments specified by an azimuthal angle, $\vartheta$, between the surface normal (z axis) and the moments and a polar angle, $\varphi$, with respect to the x axis in the plane. As seen in Fig. 6 there are very rapid changes in these angles during the first 20–30 time-steps. The main feature of this initial part of the simulation is that the $\varphi$ angles of the moments (Fig. 6, center panel) tend to arrange themselves 120° apart, i.e., at least in the lateral plane the moments immediately orient according to a 120° Néel state. This is obviously the consequence of the strong anti-ferromagnetic coupling, $J \simeq 145$ meV [50], between the Cr atoms. This ordering also serves to reduce the constraining fields (Fig. 6, right panel), initially comparable in size with $J$, by several orders of magnitudes. The evolution of the spin directions is then characterized by much slower changes whereby the $\vartheta$ angles tend to nearly 90° (Fig. 6, left panel). Beyond 2000 timesteps the moments lie, to all practical purposes, in the surface plane. Reassuringly, the slow changes seen here are accompanied by very small constraining fields clearly converging to zero. This indicates that the procedure converges indeed to a ground state of the system represented by the 120° Néel state.

While the relativistic theory we use allows us to determine the direction of the moments with respect to the lattice, the total number of timesteps calculated (~2400) was still not sufficient to achieve full convergence. In the 'final' state shown in Fig. 6 the three polar angles take the values ~75°, ~195°, and ~315°, respectively, but still they change very slowly towards the angles ~90°, ~210°, and ~330° which corresponds to the most symmetric, non-degenerate spin-configuration [51]. The cause of this extremely slow convergence is the very small in-plane magnetic anisotropy (as compared to the exchange interactions or even to the uniaxial magnetic anisotropy) which in turn results in very small constraining fields to drive the dynamics of the moments. Clearly, such a situation shows the practical limitations of first principles spin-dynamics methods without additional accelerating devices.

In order to justify that the ground state is the above mentioned most symmetric spin arrangement we used an alternative method based on the MFT, Eq. (12), where we use
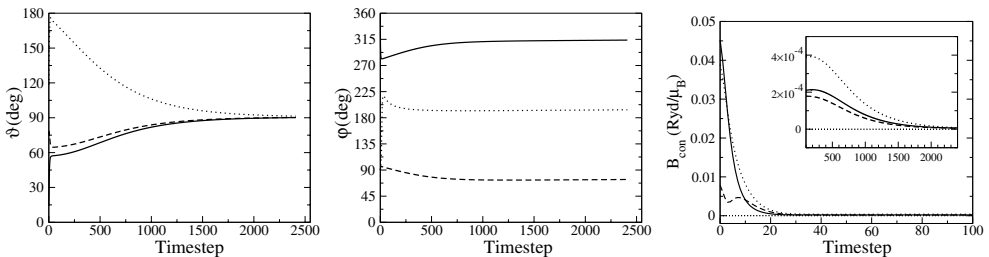


Fig. 6. Evolution of azimuthal angles (left panel) and polar angles (center panel) of the moments, as well as the magnitude of the constraining fields (right panel) from a first principles spin-dynamics simulation of a Cr trimer on Au(111). Different line styles correspond to different Cr atoms.

the potentials and fields from the end-state of our first principles spin-dynamics simulation and studied the energy as a function of the spin configuration.

In the left panel of Fig. 7 the variation of the energy is plotted for the case when the $\vartheta$ angle of all the three moments is changed from 0 to 90°, while the angles $\varphi_1 = 90°$, $\varphi_2 = 210°$, and $\varphi_3 = 330°$ are kept fixed. As expected from a simple Heisenberg model with an AFM exchange interaction, the variation of the energy closely follows a $\cos^2\vartheta$ dependence, and the state with $\vartheta = 90°$ is by about 660 meV ($\simeq -9J/2$) lower in energy than the ferromagnetic state. Next we fixed the moments in plane with $\varphi$ angles 120° apart and rotated the moments around the $z$ axis. The center panel of Fig. 7 clearly demonstrates that the 0° and the respective time-reversed state are indeed the lowest energy configurations. The magnitude of the energy change is, however, four orders of magnitude less than in the previous case, indicating the large difference between the size of the exchange interactions and the in-plane magnetic anisotropy energy. This, in turn, satisfactorily explains why the spin-dynamics simulation converged so slowly towards the ground state.

Finally, we investigated a series of spin-configurations, different from the 120° Néel state, where the direction of one moment was held at $\varphi_1 = 90°$, while the remaining two moments were rotated around the $z$ axis; one clockwise, the other one anti-clockwise. As a visualization aid, some of these configurations are depicted above the right panel of Fig. 7. As can be inferred from this panel, all the configurations under consideration are higher in energy than the Néel state. A local maximum and a global maximum can indeed be found at a collinear antiferromagnetic (state 2) and the ferromagnetic state (state 4), respectively. Apparently, the non-collinear state labeled by 3 is only about 7 meV higher in energy than the ground state. In fact, within a simple Heisenberg model, these two states are degenerate. Since the in-plane anisotropy energy is about one order magnitude smaller than this energy difference (see the middle panel of Fig. 7), the origin of the observed non-degeneracy has to be related mainly to four-spin interactions [50].

The small energy difference seen between two particular spin-states also raises the need to test the accuracy of the MFT with respect to the effective potentials and fields used. As an example we repeated the latter calculations with effective potentials and fields obtained
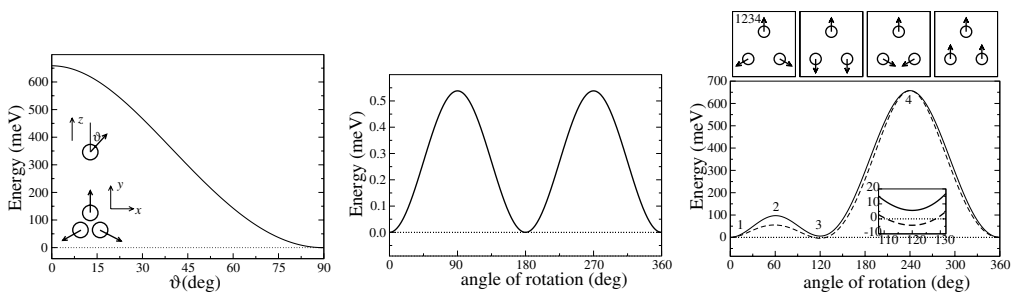


Fig. 7. Variation of the energy for different spin-configurations of a Cr trimer on Au(111) as derived from magnetic force theorem calculations based on (almost) converged effective potentials and fields of the first principles spin-dynamics simulation. Left: tilting the moments from a ferromagnetic state normal to the surface to an in-plane 120° Néel state; middle: an in-plane 120° Néel state rotated around the $z$ axis; right: one moment fixed, two moments symmetrically rotated around the $z$ axis. For this case some representative configurations are depicted above the panel and marked also in the figure at the corresponding angle of rotation. Also in this case, the energy curve obtained by using the effective potentials and fields from a self-consistent calculation with moments parallel to each other and normal to the surface is shown by dashed line (see text).

from a self-consistent calculation by setting all the moments parallel to each other and normal to the surface. The corresponding results are plotted by the dashed line in the bottom panel of Fig. 7. Apparently, there are significant differences as compared to the previous case of using the (nearly) converged potentials and fields from the SD calculation. In particular, the energy of spin-states 2 and 3 decreased in order by about 40 meV and 11 meV with respect to the Néel state. As a consequence, the energy minimum now corresponds to state 3. Since the most prominent observation of our SD simulations was a clear tendency towards Néel state[4] concluding state 3 is ground state must to be considered erroneous. This strongly indicates that one has to be careful when applying the MFT, since reliable results can only be expected by using effective potentials and fields corresponding to the real ground state (see also Ref. [12]), which then requires that one knows ahead of time what the ground state configuration is or has a way to find it.

### 3.3. Exchange mediated magnetic anisotropy (EMMA)

As we have seen above, magnetism in nanostructures can be significantly different from that of bulk system. This notwithstanding, in the previous examples, the physics that determines the final magnetic structure is also well-known in bulk materials; specifically the interplay between exchange and anisotropy in one and magnetic frustration in the second. Here, we discuss a situation where a novel physical effect manifests itself.

In previous investigations of the magnetic anisotropy of (1 1 0) nearest-neighbor (1 0 0) next-nearest-neighbor Fe-chains embedded fcc Cu, Eisenbach et al. [8] reported anisotropy energies that turned out to be competitive with the magnetostatic energy giving rise to different ground state orientations of the chain's magnetization for the two chains; along and perpendicular to the Fe-chain for (1 1 0)- and (1 0 0)-chains respectively. Although large, the actual values of the anisotropy energies (5.5 and 9.1 μRy per Fe-atom for the (1 1 0) and (1 0 0)-chains respectively) were not, however, too surprising, given the reduced, one-dimensional, symmetry of the chains. However, subsequent calculations for a (1 1 1) Fe-chain yielded an anomalously large MAE, 38 μRy, a value that is clearly out-of-line with the results for the other two orientations and normal expectations. Indeed, this finding is particularly surprising given that Fe-atoms in (1 1 0)- and (1 0 0)-chains are first and second nearest-neighbors respectively, while, for the (1 1 1)-chain, adjacent Fe-atoms are on opposite body diagonals of a cube and are only 6th nearest-neighbors. As a result the Fe-atoms are rather isolated from one another. Upon noting that an isolated Fe-impurity in Cu would see a cubic environment, intuitively, one may have expected a small anisotropy; more typical of a cubic metal.

To test this Eisenbach et al. [15] performed a fully self-consistent calculation of the magnetic anisotropy of a monatomic substitutional Fe-impurity in fcc copper. Specifically, they consider a single Fe atom replacing a Cu-atom in a periodically repeated supercell of 108 sites. The lattice constant $a$ was taken to be that of pure Cu (6.83 Bohr) and possible lattice relaxations due to the iron substitution were disregard. In determining the MAE, advantage was taken of the fact that the Fe-site has a well developed and stable magnetic moment which then polarizes surrounding Cu-sites and induces small moments on them.

---

[4] In fact, we tried several random initial configurations and all tended towards the same Néel state under FP-SD iteration.

Accordingly, the direction of the Fe-moment was constrained to lie, first along the (1 0 0) easy-direction and subsequently along the (1 1 1) hard-directions and in each case the induced moments on the Cu-sites were allowed to relax without constraint. Once again the MAE is unexpectedly large; 45.3 μRy per Fe atom. In fact, comparison with the MAE for the (1 1 1)-chain, 38 μRy, confirms that (1 1 1) Fe-chain does indeed resemble a series of isolated Fe-impurities, but now posses the question as to why the anisotropy of the isolated impurity is so large.

Insight into this is provided by Fig. 8 where we show the orientations of the induced moments for the easy and hard directions (left and right frames respectively) taken from the work of Eisenbach et al. [15]. From these figures it can be seen that the induced magnetic moments on the second neighbor Cu-sites reverse their orientation between the easy and hard directions giving rise to an exchange contribution to the magnetic anisotropy; Eisenbach et al. referred to this novel effect as exchange mediated magnetic anisotropy (EMMA).

Not only is EMMA a result of a subtle interplay between spin orbit coupling and the formation of the induced moments, but is also one that likely would have been missed using the MFT. Obviously, for the hard direction the induced moment orientations are very different from what would be obtained by a rigid rotation of the moments of the easy direction. Thus, the influence of self-consistently on the magnetic anisotropy is substantial and can not be neglected. To illustrate this, we have calculated the MAE using the FPA approximation and a configuration where the directions of all the induced moments are rigidly rotated with the Fe moment. For this, we find a MAE of only 0.05 μRy per Fe-atom, i.e. the order of magnitude that would be intuitively expected, and one that is comparable to the value we obtain for bulk bcc Fe (0.06 μRy per Fe-atom). On the other hand, a FPA calculation performed using the potentials we have found for the easy direction, but
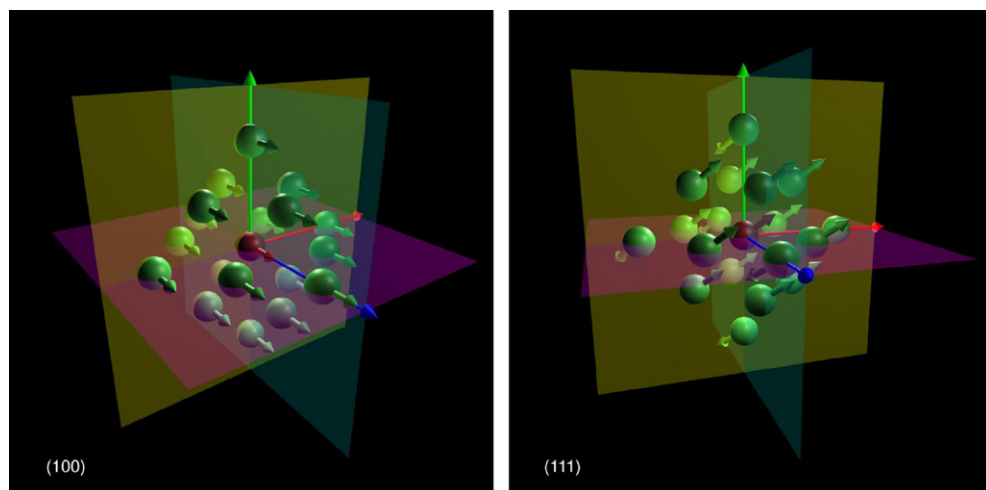


Fig. 8. The induced magnetic moment directions (green) on the first and second nearest neighbour shells surrounding the Fe impurity (red) for the easy 1 0 0 direction (left) and the hard 1 1 1 direction (right). The magnitude of the moments are not shown. Notice the switch in the direction of the second shell Cu moments. (For interpretation of the references in color in this figure legend, the reader is referred to the web version of this article.)

using the self-consistently calculated moment directions for the hard direction, we find the much larger MAE of 10.3 μRy per Fe-atom. While this calculation will not properly take into account the change in Fe d–Cu p hybridization, it clearly shows the importance of the fully self-consistent treatment of magnetic moments and their direction.

## 4. Conclusions

Taken together the nanostructures that we have presented results for illustrate the need to treat the underlying electronic interactions on a fully self-consistent basis in which the very different energy scales appropriate to exchange coupling ($\sim$1 mRy) and magneto-crystalline anisotropy ($\sim$1 μRy) are treated on an equal footing. In the case of Co-chains adjacent to a Pt{1 1 1}-surface step-edge the interplay between exchange interactions and anisotropy results in a non-intuitive angle of tilt of the Co-moments relative to the Pt step edge but one that can be readily understood in terms of the underlying anisotropy constants which, in this case, can be obtained using the frozen potential approximation [12,14] once the ground state configuration is known. For the Cr-trimer, due to the in-plane anisotropy being very small, two very different orientational states are energetically competitive and fully self-consistent calculations are needed in order to identify the actual ground state. Studies of Fe-chains embedded in Cu reveal an unexpectedly high MAE for chains oriented along the 1 1 1-direction; compared with those oriented along the 1 1 0- and 1 0 0-directions. Further calculations for an isolated Fe-impurity trace this anomaly to an exchange like contribution resulting from the interaction of the Fe-impurity with induced moments on surrounding Cu-sites [15].

## Acknowledgements

## References

[1] Kübler J. J Phys: Condens Matter 2003;15:V21.
[2] Aharoni A. Introduction to the theory of magnetism. Oxford: Oxford Science Publications; 2000.
[3] Brown WF. Micromagnetics. New York: Interscience; 1963.
[4] T. Gilbert, Armour research foundation, report no. 11, Illinois Institute of Technology; 1955.
[5] Gilbert TL. Phys Rev 1955;100:1243.
[6] Ujfalussy B, Lazarovits B, Szunyogh L, Stocks GM, Weinberger P. Phys Rev B 2004;70:100404(R).
[7] Lazarovits B, Újfalussy B, Szunyogh L, Stocks GM, Weinberger P. J Phys: Condens Matter 2004;16:S5833.
[8] Eisenbach M, Györffy BL, Stocks GM, Újfalussy B. Phys Rev B 2002;65:144424.
[9] Anton J, Fricke B, Engel E. Phys Rev A 2004;69:012505.

[10] Szunyogh L, Újfalussy B, Weinberger P. Phys Rev B 1995;51:9552.

[11] Lazarovits B, Szunyogh L, Weinberger P. Phys Rev B 2002;65:104441.

[12] Jansen HJ. Phys Rev B 1999;59:4699.

[13] Pettifor DG. Commun Phys 1976;1:141.

[14] Nicholson DMC, Brown RH. Phys Rev B 2003;67:16401.

[15] M. Eisenbach, G.M. Stocks, B.L. Györffy, unpublished.

[16] Hohenberg P, Kohn W. Phys Rev 1964;136 B:864.

[17] Kohn W, Sham LJ. Phys Rev 1965;140 A:133.

[18] von Barth U, Hedin L. J Phys C 1972;5:1629.

[19] Dreizler RM, Gross EKU. Density functional theory. Heidelberg: Springer Verlag; 1990.

[20] Rajagopal AK, Callaway J. Phys Rev B 1973;7:1912.

[21] MacDonald AH, Vosko SH. J Phys C 1979;12:2977.

[22] Rajagopal AK. J Phys C 1978;11:L943.

[23] Eschrig H, Seifert G, Ziesche P. Solid State Commun 1985;56:777.

[24] Antropov VP, Katsnelson MI, van Schilfgaarde M, Harmon BN. Phys Rev Lett 1995;75:729.

[25] Antropov VP, Katsnelson MI, Harmon BN, van Schilfgaarde M, Kusnezov D. Phys Rev B 1996;54:1019.

[26] Niu Q, Wang X, Kleinman L, Liu W-M, Nicholson DMC, Stocks GM. Phys Rev Lett 1999;83:207.

[27] Capelle K, Vignale G, Györffy BL. Phys Rev Lett 2001;87:206403.

[28] Capelle K, Györffy BL. Euro Phys Lett 2003;61:354.

[29] These ideas provide the underpinning of the fist principles mean field disordered local moment (DLM) approach for studying metals above their Curie temperature and of the magnetic phase transition. For a discussion see: Györffy BL et al. J Phys F – Metal Phys 1985;15:1337.

[30] Stocks GM, Újfalussy B, Wang X, Nicholson DMC, Shelton WA, Wang Y, Canning A, Györffy BL. Philos Mag B 1998;78:665.

[31] Újfalussy B, Wang X, Nicholson DMC, Shelton WA, Stocks GM, Wang Y, Györffy BL. J Appl Phys 1999;85:4824.

[32] Dederichs PH, Blügel S, Zeller R, Akai H. Phys Rev Lett 1984;53:2512.

[33] Györffy B, Stott MJ. In: Fabian DJ, Watson LM, editors. Band structure spectroscopy of metals and alloys. Academic; 1972.

[34] Faulkner SJ, Stocks GM. Phys Rev B 1980;21:3222.

[35] Korringa J. Physica 1947;13:392.

[36] Kohn W, Rostoker N. Phys Rev 1954;94:1111.

[37] Wang Yang, Stocks GM, Shelton WA, Nicholson DMC, Szotek Z, Temmerman WM. Phys Rev Lett 1995;75:2867.

[38] Gambardella P, Dallmeyer A, Maiti K, Malagoli MC, Eberhardt W, Kern K, Carbone C. Nature 2002;416:301.

[39] Gambardella P. J Phys: Condens Matter 2003;15:S2533.

[40] Shick A, Máca F, Oppeneer PM. Phys Rev B 2004;69:212410.

[41] Baud S, Ramseyer Ch, Bihlmayer G, Blügel S. Phys Rev B 2006;73:104427.

[42] Kawamura H. J Phys: Condens Matter 1998;10:4707.

[43] Fazekas P. Lecture notes on electron correlation and magnetism. Series in modern condensed matter physics, vol. 5. Singapore: World Scientific; 1999 and references therein.

[44] Kurz Ph, Bihlmayer G, Hirai K, Blügel S. Phys Rev Lett 2001;86:1106.

[45] Kohl C, Bertsch GF. Phys Rev B 1999;60:4205.

[46] Hobbs D, Kresse G, Hafner J. Phys Rev B 2000;62:11556.

[47] (a) Uzdin S, Uzdin V, Demangeat C. Comp Mater Sci 2000;17(441):441;
(b) Uzdin S, Uzdin V, Demangeat C. Surf Sci 2001;482–485:965.

[48] A. Bergman, L. Nordström, A.B. Klautau, S. Frota-Pessôa, O. Eriksson, cond-mat/0511542; 2005.

[49] Jamnelea T, Madhavan V, Crommie MF. Phys Rev Lett 2001;87:256804.

[50] Lazarovits B, Simon P, Zaránd G, Szunyogh L. Phys Rev Lett 2005;95:077202.

[51] In fact, due to time-reversal invariance, this configuration is doubly degenerate with the state described by $\varphi_1 = 270°$, $\varphi_2 = 30°$, and $\varphi_3 = 150°$.